

Hybrid Model Predictive Control of the Step-Down DC-DC Converter

Tobias Geyer, Georgios Papafotiou, *Member, IEEE*, and Manfred Morari, *Fellow, IEEE*

Abstract—Dc-dc converters pose challenging hybrid control problems, since the semiconductor switches induce different modes of operation and several constraints (on the duty cycle and the inductor current) are present. In this paper, we propose a novel approach to the modelling and controller design problem for fixed-frequency dc-dc converters, using a synchronous step-down dc-dc converter as an illustrative example. We introduce a hybrid converter model that is valid for the whole operating regime. Based on this model, we formulate and solve a constrained optimal control problem. To make the scheme implementable, we derive off-line the explicit state-feedback control law, which can be easily stored and implemented in a look-up table. A Kalman filter is added to account for unmeasured load variations and to achieve zero steady-state output voltage error. An a posteriori analysis proves – by deriving a piecewise quadratic Lyapunov function – that the closed-loop system is exponentially stable. Simulation results demonstrate the potential advantages of the proposed control methodology.

Index Terms—Model predictive control, hybrid system, piecewise affine system, dc-dc converter, power electronics.

I. INTRODUCTION

Nowadays, switch-mode dc-dc conversion is a mature and well-established technology, used in a large variety of demanding applications. Yet, the control problems associated with such converters still pose theoretical challenges for academic researchers, which manifest themselves in the numerous publications on this subject over the last years. The development of advanced control techniques together with the increased computational power of the available hardware in the control loop, allow tackling the control problem from a new perspective. In this paper, we propose a new approach to the problem – namely, we pose and solve the constrained optimal control problem for fixed-frequency switch-mode dc-dc converters.

The difficulties in controlling dc-dc converters arise from their hybrid nature. In general, these converters feature three different modes of operation, where each mode has an associated linear continuous-time dynamic. Furthermore, constraints are present, which result from the converter topology. In particular, the manipulated variable of the control problem (the duty cycle) is bounded between zero and one, and in the discontinuous current operation a state (inductor current) is constrained to be nonnegative. Additional constraints may

be imposed as safety measures, such as current limiting or soft-starting, where the latter constitutes a constraint on the maximal derivative of the current during start-up. The control problem is further complicated by gross changes in the operating point that occur due to input voltage and output load variations.

Motivated by the aforementioned difficulties, we present a novel approach to the modelling and controller design problem for fixed-frequency dc-dc converters, using a synchronous step-down converter as an illustrative example. The converter is modelled as a hybrid system. A piecewise affine (PWA) model is derived that is valid for the whole operating regime and captures the evolution of the state variables within the switching period. Based on the hybrid model, we formulate a constrained finite time optimal control (CFTOC) problem, which is solved off-line using Dynamic Programming [1]. This approach leads to a state-feedback controller that is defined over the whole state-space and yields the duty cycle as a PWA function of the states. This controller can be implemented in form of a look-up table, thus avoiding on-line optimization. We would like to emphasize that the controller is designed such that for the control law computation only directly available quantities are needed. In particular, we assume that – in accordance with common practice – the input voltage, the inductor current and the output voltage can be directly measured.

The proposed approach carries a number of benefits – the most prominent being the systematic character of the design procedure that avoids excessive iterations and tuning. In particular, the control objectives are expressed in the cost function of the CFTOC in a straightforward manner, and all constraints are directly included in the design procedure leading to a controller that achieves current limiting without adopting the traditional implementation. Most importantly, the control law covers the whole operating regime due to the derived PWA model that provides an accurate representation of the converter for the whole state-input space. This leads to a closed-loop performance independent from the operating point. Moreover, in an a posteriori step, a piecewise quadratic (PWQ) Lyapunov function is derived, which proves that the derived controller is exponentially stable (at least for the nominal values of the input voltage and the load). Furthermore, the proposed control scheme rejects gross disturbances in the (measured) input voltage and the (unmeasured) output resistance.

These benefits, however, come at a cost. The derived controller is rather complex and the look-up table can easily feature 100 or more entries. In some applications this may prove to be a limiting factor. Yet, the main scope of this paper is to illustrate that the application of advanced hybrid

This work was done at the Automatic Control Laboratory, ETH Zurich, 8092 Zurich, Switzerland

T. Geyer is currently with GE Global Research Europe, Munich, Germany, geyer@control.ee.ethz.ch

G. Papafotiou is currently with ABB Corporate Research, Dättwil, Switzerland, georgios.papafotiou@ch.abb.com

M. Morari is with the Automatic Control Laboratory, ETH Zurich, Switzerland, morari@control.ee.ethz.ch

optimal control methods for dc-dc converters is conceivable and within reach. Moreover, compared with only locally valid controllers, which are predominantly used as shown below, a more complex solution is to be expected since the control problem is addressed for the complete state-space.

Due to space limitations, we provide here only a brief overview of the literature most related to our approach – a more extensive coverage can be found in Section 8.1.2 of [2]. The dominant approach to the modelling and controller design of switch-mode dc-dc converters is the method of state-space averaging [3], [4] and the design of a control loop comprising a PI-type controller and a Pulse Width Modulation (PWM) unit. The controller is tuned for a model locally linearized around a specific operating point. In the literature a wide range of strategies have been proposed for improving the controller design, but the majority of the proposed design methods is still based on averaged and/or locally linearized models of the converters. In this category, the methods introduced vary from Fuzzy Logic [5] to Linear Quadratic Regulators (LQR) [6], and from non-linear control techniques [7], [8], [9] to feedforward control [10], [11].

In [12], [13], the authors propose an (unconstrained) LQR controller based on a locally linearized discrete-time model of the averaged dc-dc converter. In [14], an unconstrained nonlinear predictive controller is formulated for a dc-dc converter using a control methodology that extends the concept of Generalized Predictive Control [15] to nonlinear systems. For the latter, an implementation may prove to be difficult due to the lack of convergence guarantees and the potentially excessive computation time. As an unconstrained optimization problem is solved, the constraints on the duty cycle and the inductor current cannot be handled in a straightforward manner.

Recently, there have been several proposals to apply new results from hybrid system theory to the analysis and controller design of dc-dc converters. In [16] and [17], the authors consider the switch position as the boolean manipulated variable of the control problem, and synthesize stabilizing controllers using Relaxed Dynamic Programming [16] and Lyapounov theory. Our approach, on the other hand, uses the duty cycle, a continuous-valued real variable bounded by 0 and 1, as the manipulated variable, thus ensuring a constant switching frequency. In any case, our approach is more related to [18], with the main differences that we address the constraints on the state and input variables during the controller design, and the fact that the controller is based on a PWA description of the converter, which is valid for the whole operating range.

The paper is organized in the following way. We start in Section II by summarizing the nonlinear continuous-time state-space equations of the converter. The ν -resolution modelling approach is introduced and analyzed in Section III. Based on this model, we formulate and solve a constrained finite time optimal control problem in Section IV. In Section IV-C we pre-solve the control problem off-line and derive the equivalent state-feedback control law parameterized over the state-space. This controller can be stored in a look-up table, hence allowing the practical implementation of the proposed control scheme. A piecewise quadratic (PWQ) Lyapunov function is derived

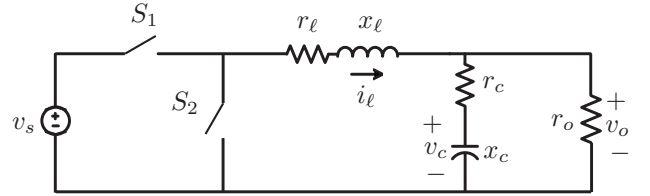


Fig. 1: Topology of the step-down synchronous converter

in Section V proving that the nominal closed-loop system is exponentially stable. Section VI illustrates various aspects of the system's behavior with simulation results including start-up, a comparison with a current mode PI controller, and gross changes in the input voltage and the output resistance. The paper is summarized in Section VII and conclusions are drawn.

II. MATHEMATICAL MODEL OF SYNCHRONOUS CONVERTER

We start by modelling the physical behavior of the synchronous step-down converter in continuous-time, and derive for each mode of operation the state-space equations. This model will be used later to simulate the behavior of the plant. The circuit topology of the converter is shown in Fig. 1. Using normalized quantities, r_o denotes the output load, which we assume to be ohmic, r_c is the Equivalent Series Resistance (ESR) of the capacitor, r_l is the internal resistance of the inductor, x_l and x_c represent the inductance and the capacitance of the low-pass filtering stage, respectively, and v_s denotes the input voltage. The semiconductor switches, which are operated dually, are driven by a pulse sequence with a constant switching frequency f_s (period T_s). The duty cycle d is defined by $d = \frac{t_{on}}{T_s}$, where t_{on} represents the interval within the switching period during which the primary switch is in conduction. For every switching period k the duty cycle $d(k) \in [0, 1]$ is chosen by the controller.

We define $x(t) = [i_l(t) \ v_c(t)]^T$ as the state vector, where $i_l(t)$ is the inductor current and $v_c(t)$ the capacitor voltage. Given the duty cycle $d(k)$ during the k -th period, the system is described by the following set of affine continuous-time state-space equations. While S_1 is conducting, they are given by

$$\frac{dx(t)}{dt} = Fx(t) + fv_s, \quad kT_s \leq t < (k + d(k))T_s, \quad (1)$$

and when S_1 is off, the system evolves autonomously according to

$$\frac{dx(t)}{dt} = Fx(t), \quad (k + d(k))T_s \leq t < (k + 1)T_s, \quad (2)$$

where the matrices F and f are given by

$$F = \begin{bmatrix} -\frac{1}{x_l} \left(r_l + \frac{r_o r_c}{r_o + r_c} \right) & -\frac{1}{x_l} \frac{r_o}{r_o + r_c} \\ \frac{1}{x_c} \frac{r_o}{r_o + r_c} & -\frac{1}{x_c} \frac{1}{r_o + r_c} \end{bmatrix} \quad (3)$$

and

$$f = \begin{bmatrix} \frac{1}{x_l} \\ 0 \end{bmatrix}, \quad (4)$$

respectively. The output voltage $v_o(t)$ across the load r_o is expressed as a function of the states through

$$v_o(t) = g^T x(t) \quad (5)$$

with

$$g = \begin{bmatrix} \frac{r_o r_c}{r_o + r_c} & \frac{r_o}{r_o + r_c} \end{bmatrix}^T. \quad (6)$$

Of main interest from a control point of view is the output voltage error

$$v_{o,err}(k) = \frac{1}{T_s} \int_{kT_s}^{(k+1)T_s} (v_o(t) - v_{o,ref}) dt \quad (7)$$

integrated over the k -th switching period, where $v_{o,ref}$ denotes the reference of the output voltage.

The converter model includes constraints. By definition, the duty cycle $d(k)$ is constrained between zero and one. Moreover, a current limiting constraint has to be accounted for, which is given by $-i_{\ell,max} < i_{\ell}(t) < i_{\ell,max}$.

In general, the parameters of a dc-dc converter are time-varying. These variations can be divided into two categories. The parameters of the low-pass filtering stage are subject only to slow deterioration over time or temperature changes. Specifically, these include the ESR of the capacitor r_c , the internal resistance of the inductor r_{ℓ} , and the inductance and capacitance of the low-pass filtering stage x_{ℓ} and x_c , respectively. On the other hand, the input voltage v_s and the load resistance r_o may vary step-wise and significantly. In particular the load resistance may vary by several orders of magnitude ranging from a short circuit to open circuit conditions.

III. MODELLING FOR CONTROLLER DESIGN

In the following, we derive a model to serve as prediction model for the optimal control problem formulation in Section IV. For this, we reformulate the converter model and introduce the ν -resolution modelling approach.

A. Reformulated Continuous-Time Model

First, from an implementation point of view, it is preferable that all states are directly measurable. Thus, we replace in the state vector the capacitor voltage by the output voltage¹. This leads to the redefined state vector $x(t) = [i_{\ell}(t) \ v_o(t)]^T$, and the matrices F , f and g turn into

$$F = \begin{bmatrix} -\frac{r_{\ell}}{x_{\ell}} & -\frac{1}{x_{\ell} + r_c r_o x_c} \\ r_o \frac{x_{\ell} - r_c r_{\ell} x_c}{(r_o + r_c) x_c x_{\ell}} & -\frac{x_{\ell}}{(r_o + r_c) x_c x_{\ell}} \end{bmatrix}, \quad (8)$$

$$f = \begin{bmatrix} \frac{1}{x_{\ell}} \\ \frac{r_o}{r_o + r_c} \frac{r_c}{x_{\ell}} \end{bmatrix}, \quad g = \begin{bmatrix} 0 & 1 \end{bmatrix}^T.$$

Second, as will be motivated later, we remove v_s from the model equations by using it to scale² the physical quantities (states, output voltage reference and current limit) used in the

¹In general, such a substitution is not advisable, since the output voltage of most dc-dc converters is not continuous over time. For the step-down converter treated here, however, the output voltage is a continuous function of time.

²As it is common practice, we assume all quantities to be given in the p.u. system, thus to be normalized in the standard sense. The reader should distinguish between the p.u. normalization and the scaling over v_s .

model. Therefore, we introduce the state $x'(t) = \frac{x(t)}{v_s}$, which scales (1), (2), (5) and (7) over v_s . This yields the reformulated state-space equations

$$\frac{dx'(t)}{dt} = \begin{cases} Fx'(t) + f, & kT_s \leq t < (k + d(k))T_s \\ Fx'(t), & (k + d(k))T_s \leq t < (k + 1)T_s \end{cases} \quad (9a)$$

$$v'_o(t) = g^T x'(t), \quad (9b)$$

where the matrices F , f and g are as in (8), and $v'_o = \frac{v_o}{v_s}$ is the scaled output voltage. The relation for the output voltage error is given by

$$v'_{o,err}(k) = \frac{1}{T_s} \int_{kT_s}^{(k+1)T_s} (v'_o(t) - v'_{o,ref}) dt \quad (10)$$

with the scaled output voltage reference $v'_{o,ref} = \frac{v_{o,ref}}{v_s}$ and the scaled output voltage error $v'_{o,err} = \frac{v_{o,err}}{v_s}$. Furthermore, we normalize the current limit to

$$i'_{\ell,max} = \frac{i_{\ell,max}}{v_s}. \quad (11)$$

Strictly speaking the above scaling in (9) holds only if v_s is time-invariant (or piecewise constant). Nevertheless, for the prediction model one only needs to assume that the input voltage remains constant within the limited time of the prediction interval (a few switching periods). Since in practice the input voltage is either piecewise constant or varies only slowly compared to the (very short) switching period, the normalized state equations can serve as a sufficiently accurate prediction model.

Before proceeding, we elaborate on the parameters of the reformulated model. For the controller design, we assume that (the slowly varying parameters) r_c , r_{ℓ} , x_{ℓ} and x_c are constant. Moreover, we additionally assume that the load resistance r_o is constant³, but the input voltage v_s may vary with time. Since the scaling renders the prediction model equations independent of (the time-varying) v_s , the matrices F , f and g in (8) are time-invariant. Hence, the only time-varying model parameters are the scaled output voltage reference $v'_{o,ref}$ and the scaled current limit $i'_{\ell,max}$.

B. ν -Resolution Discrete-Time Hybrid Model

Using the reformulated continuous-time model derived in the previous section as a starting point, the goal of this section is to derive a model of the converter that is suitable to serve as a prediction model for the optimal control problem. This model should have the following properties. First, it is natural to formulate the model and the controller in the discrete-time domain, as the manipulated variable given by the duty cycle is constant within the switching period and changes only at the time-instants kT_s , $k \in \mathbb{N}_0$. Second, it would be beneficial to capture the evolution of the states also within the switching period, as this would enable us to impose constraints on the states not only at time-instants kT_s but also on intermediate samples. This is needed to keep the peaks of the inductor

³In Section IV-D, we will relax this assumption and introduce a Kalman filter to account for (unmeasured) changes in r_o by manipulating the scaled output voltage reference $v'_{o,ref}$.

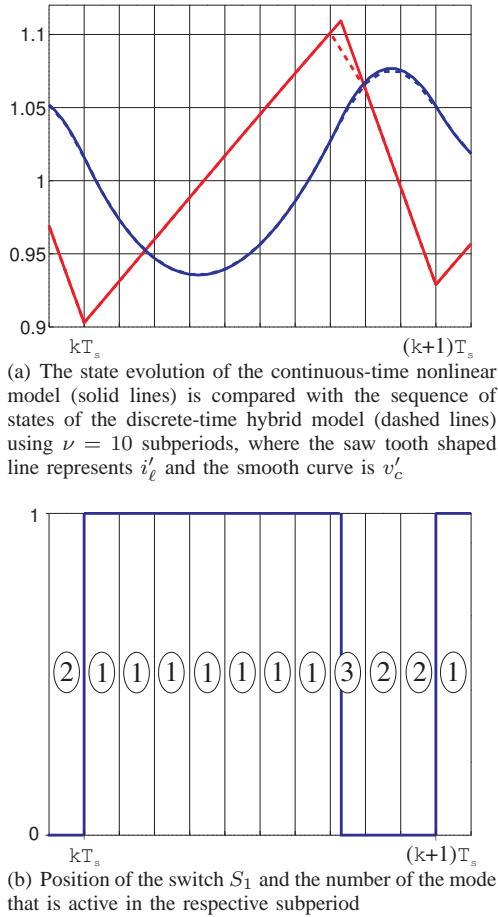


Fig. 2: The ν -resolution modelling approach visualized for the k -th period

current below the current limit. Third, the model needs to yield an approximation of the output voltage error given by the integral (10). Most important, as the converter is intrinsically hybrid in nature, we aim to retain the structure of the two operation modes and to account for the hybrid character.

Hereafter, we introduce the ν -resolution modelling approach that accounts for all the above requested properties. As illustrated in Fig. 2, the basic idea is to divide the period of length T_s into ν *notional subperiods* of length $\tau_s = T_s/\nu$ with $\nu \in \mathbb{N}$, $\nu \geq 1$. Within the k -th period, we use $\xi(n)$ to denote the states at time-instants $kT_s + n\tau_s$ with $n \in \{0, 1, \dots, \nu\}$. Furthermore, by definition, $\xi(0) = x'(k)$ and $x'(k+1) = \xi(\nu)$ hold. Note that ξ refers to the scaled x' .

We would like to stress that the controller samples the physical plant only every T_s . Subdividing T_s into subperiods does *not* imply a higher sampling rate. The ν -resolution approach increases the model accuracy beyond standard averaging while retaining the sampling interval T_s .

Next, we introduce ν binary variables

$$\sigma_n = \text{true} \iff d(k) \geq \frac{n}{\nu}, \quad n = 0, \dots, \nu - 1, \quad (12)$$

which represent the switch positions of S_1 at time-instants $n\tau_s$. Recall that the switch S_2 is dually operated with respect to S_1 .

For each subperiod, we introduce the two modes discussed above (switch closed and open, respectively) plus an additional

third (auxiliary) mode that captures the transition from mode one to mode two. More specifically, the modes are (i) the switch S_1 remains closed for the whole subperiod, (ii) the switch S_1 is open for the whole subperiod, and (iii) the switch S_1 is opening within the subperiod. Hence, for the n -th subperiod, the state-update equation is

$$\xi(n+1) = \begin{cases} \Phi \xi(n) + \Psi, & \sigma_n \wedge \sigma_{n+1} \\ \Phi \xi(n), & \bar{\sigma}_n \\ \Phi \xi(n) + \Psi(\nu d(k) - n), & \sigma_n \wedge \bar{\sigma}_{n+1}, \end{cases} \quad (13)$$

where Φ and Ψ are the discrete-time representations of F and f as defined in (8) with “sampling” time τ_s . Note that if the third mode is active, i.e. $\sigma_n \wedge \bar{\sigma}_{n+1}$ holds, $\nu d(k) - n$ is bounded by zero and one. Thus, the third mode is a weighted average of the modes one and two. By increasing ν the error introduced by averaging can be made arbitrarily small.

The safety current limit is imposed on the evolution of the states $\xi(n)$ by adding the constraints

$$-i'_{\ell, \max} \leq [1 \ 0] \xi(n) \leq i'_{\ell, \max}, \quad n = 0, 1, \dots, \nu - 1. \quad (14)$$

The notion of the ν -resolution modelling thus allows us to impose the current limit on the states $\xi(n)$ with the fine resolution $\frac{T_s}{\nu}$ rather than only on the states $x'(k)$ with the coarse resolution T_s .

Using the output voltage given by

$$v'_o(n) = g^T \xi(n), \quad (15)$$

we approximate the voltage error integral (10) for the k -th period in the following way.

$$v'_{o, \text{err}}(k) = \sum_{n=0}^{\nu-1} \frac{v'_o(n) + v'_o(n+1)}{2\nu} - v'_{o, \text{ref}} \quad (16)$$

Before proceeding, we define constraints on the states, the parameters and the duty cycle. For the states, we require $x' \in \mathcal{X}'$, and the parameter vector $v'_p = [v'_{o, \text{ref}} \ i'_{\ell, \max}]^T$ is restricted to $v'_p \in \mathcal{V}'$, where \mathcal{V}' is application specific. The duty cycle, on the other hand, is physically restricted to $d \in \mathcal{U} = [0, 1]$.

In summary, the ν -resolution modelling approach provides a description of the state evolution within one period. In particular, the discrete-time sequence $[\xi(0), \xi(1), \dots, \xi(\nu)]$ is an accurate representation of the continuous-time evolution of $x'(t)$ for $t \in [kT_s, (k+1)T_s]$. The only approximation introduced is the weighted average that appears in the third mode of (13) when switch S_1 is turned off.

C. Formulation of ν -Resolution Model in Hybrid Frameworks

1) *MLD Form*: Using the HYbrid Systems DEscription Language HYSDEL [19], the above described model can be easily cast in the Mixed Logical Dynamical (MLD) framework [20], which is well-suited for constrained optimal control.

The general MLD form is

$$x(k+1) = Ax(k) + B_1u(k) + B_2\delta(k) + B_3z(k) \quad (17a)$$

$$y(k) = Cx(k) + D_1u(k) + D_2\delta(k) + D_3z(k) \quad (17b)$$

$$E_2\delta(k) + E_3z(k) \leq E_4x(k) + E_1u(k) + E_5, \quad (17c)$$

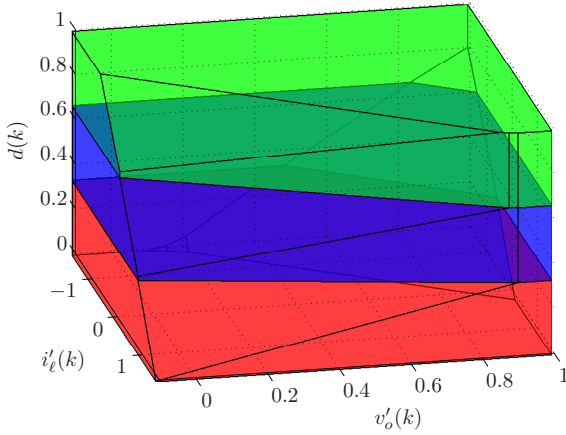


Fig. 3: Polyhedral partition of the converter's PWA model for $\nu = 3$ (for the converter parameters in Table I, intersected with $v'_{o,ref} = 0.556$ p.u. and $i'_{l,max} = 1.667$ p.u.)

where $x \in \mathbb{R}^{n_c} \times \{0, 1\}^{n_\ell}$ denotes the states, $u \in \mathbb{R}^{m_c} \times \{0, 1\}^{m_\ell}$ the inputs and $y \in \mathbb{R}^{p_c} \times \{0, 1\}^{p_\ell}$ the outputs, with both real and binary components. Furthermore, $\delta \in \{0, 1\}^{r_\ell}$ and $z \in \mathbb{R}^{r_c}$ represent binary and auxiliary continuous variables, respectively. These variables are introduced when translating propositional logic or PWA functions into linear inequalities. All constraints on states, inputs, outputs and auxiliary variables are summarized in the mixed-integer linear inequality constraint (17c). For details on the MLD framework, the reader is referred to [20].

The ν -resolution model (12)–(16) can be directly described in HYSDEL on a high-level textual basis. For the HYSDEL code the interested reader is referred to Appendix A.4 in [2]. The derivation of the MLD model (17) is performed by the HYSDEL compiler, which generates the corresponding matrices. The above procedure yields an MLD model with two states, two parameters, (7ν) z -variables, $(2(\nu - 1) + 1)$ δ -variables and $(24\nu + 8)$ mixed-integer linear inequality constraints.

2) *PWA Form*: For the computation of the explicit state-feedback control law, the converter model is required to be in PWA form. Polyhedral PWA systems are defined by partitioning the state-space into polyhedra and associating with each polyhedron an affine state-update and output function [21]. As shown in [22], for a given well-posed MLD model there exists always an *equivalent* PWA representation. Equivalence implies, that for all feasible initial states and for all feasible input trajectories, both models yield the same state and output trajectories. The conversion from MLD to PWA form is performed efficiently using the mode enumeration algorithm presented in [23]. The resulting PWA model is defined on the five-dimensional space $\mathcal{X}' \times \mathcal{V}' \times \mathcal{U}$ given by the states, the parameters and the input.

Example 1: To visualize the PWA model of the converter, consider the set of converter parameters given in Table I. Furthermore, we set $\mathcal{X}' = [-4, 4] \times [-0.1, 1]$ p.u., $\mathcal{V}' = [0.2, 1] \times [0.6, 3]$ p.u. and $\mathcal{U} = [0, 1]$. To better visualize the polyhedral partition, we perform an intersection of $\mathcal{X}' \times \mathcal{V}' \times \mathcal{U}$ with $v'_{o,ref} = 0.556$ p.u. and $i'_{l,max} = 1.667$ p.u. thus

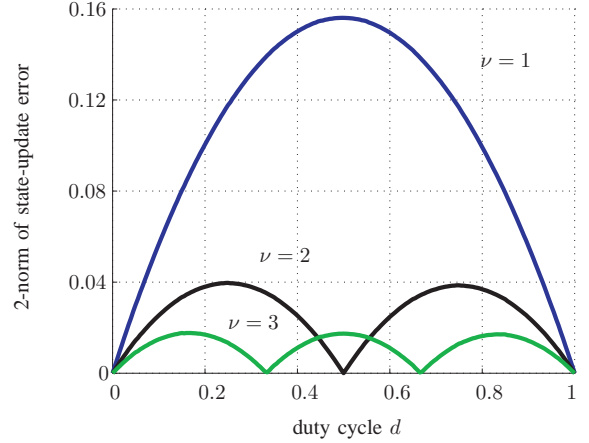


Fig. 4: Accuracy (2-norm error) of the state-update function of the ν -resolution model with respect to the nonlinear dynamic

removing the two dimensions corresponding to the parameter space \mathcal{V}' . Fig. 3 shows the resulting polyhedral partition of the state-input space $\mathcal{X}' \times \mathcal{U}$, where we have additionally restricted the first state i'_l to $[-i'_{l,max}, i'_{l,max}]$. Note that small (large) capacitor voltages and large (small) duty cycles correspond to large (small) inductor currents. Since we have added the upper and lower safety current constraint in (14) as hard constraints to the model, these state-input combinations are removed from the $\mathcal{X}' \times \mathcal{V}' \times \mathcal{U}$ space.

D. Analysis of Hybrid Model

The exact discrete-time mapping from time-instant kT_s to $(k + 1)T_s$ yields the nonlinear state-update map

$$x'_{exact}(k + 1) = e^{FT_s} x'(k) + \int_0^{d(k)T_s} e^{F(T_s-t)} dt f, \quad (18)$$

which is the discrete-time representation of (9a). The error between (18) and the state-update function of the ν -resolution model is defined as

$$e(d) = x'_{exact}(k + 1) - x'(k + 1). \quad (19)$$

The 2-norm of this error is plotted in Fig. 4 as a function of the duty cycle for $\nu = 1, 2, 3$ using the set of converter parameters of Table I. As can be easily shown analytically by applying (13) consecutively the error $e(d)$ is a function of the duty cycle only. Hence, since $e(d)$ is independent of the state $x'(k)$, this comparison holds for the whole state-space.

The choice of $\nu = 1$ yields the standard (discrete-time) averaged model, which is predominately used for the controller design of dc-dc converters.

$$x'(k + 1) = \Phi x'(k) + \Psi d(k) \quad (20)$$

with $\Phi = e^{FT_s}$ and $\Psi = \int_0^{T_s} e^{F(T_s-t)} dt f$. Obviously, the averaged model is perfectly accurate for $d(k) = 0$ and $d(k) = 1$, and it is at its worst for $d(k) = 0.5$. As one can see, setting ν to 2 already significantly improves the accuracy of the model. For $\nu = 3$, the error is small enough to allow designing a controller with sufficiently accurate closed-loop performance.

Using (13) consecutively, the discrete-time state-update map of the ν -resolution model can be derived. For $\nu = 3$, this is

$$x'(k+1) = \Phi^3 x'(k) + \begin{cases} \Phi^2 \Psi 3d(k), & d(k) \in [0, \frac{1}{3}] \\ \Phi^2 \Psi + \Phi \Psi 3(d(k) - \frac{1}{3}), & d(k) \in [\frac{1}{3}, \frac{2}{3}] \\ \Phi^2 \Psi + \Phi \Psi + \Psi 3(d(k) - \frac{2}{3}), & d(k) \in [\frac{2}{3}, 1] \end{cases}, \quad (21)$$

with $\Phi = e^{F\tau_s}$, $\Psi = \int_0^{\tau_s} e^{F(\tau_s-t)} dt f$ and $\tau_s = \frac{T_s}{3}$. Note that for the ν -resolution model, the matrices Φ and Ψ have been derived by exact time-discretization over the subperiod τ_s .

The partition induced by this map confirms the polyhedral partition of the PWA ν -resolution model, which is visualized in Fig. 3. As the converter dynamics are linear in the states, there is no partitioning in the state-space. Yet, they are nonlinear in the duty cycle. The ν -resolution model approximates this nonlinearity by partitioning the duty cycle in ν segments and by averaging the transition from the first to the second mode by a third (auxiliary) mode. In particular, the hybrid model is continuous when moving from one polyhedron to a neighboring one. This follows from the state-update equation (21) and is confirmed by the continuity in Fig. 4.

We would like to stress once more that these results hold for the whole state-space making the model a valid approximation for all operating points, rather than locally for a specific operating point, as standard linearization would do. The trade-off between model accuracy and complexity is determined by the design parameter ν .

IV. CONSTRAINED OPTIMAL CONTROL

In this section, we propose a new optimal control scheme for dc-dc converters. Our controller is based on constrained finite-time optimal control (CFTOC) with a receding horizon policy, more specifically on Model Predictive Control (MPC) [24]. In MPC, the control input is obtained by solving at each sampling instant an open-loop optimal control problem over a finite horizon using the current state of the plant as the initial state. The underlying optimization procedure yields an optimal control sequence that minimizes a given objective function. By only applying the first control input in this sequence and by recomputing the control sequence at the next sampling instant, a receding horizon policy is achieved, which provides feedback. A major advantage of MPC is its ability to cope with hard constraints on manipulated variables, states and outputs. Furthermore, as introduced in [20], MLD models can be straightforwardly used as prediction models for MPC. Moreover, the optimal state-feedback control law can be pre-computed off-line for all feasible states using the state vector as a parameter. For hybrid systems, such a method has been introduced recently [25]. Apart from this, to address unmeasured changes in the load resistor, we introduce at the end of this section a Kalman filter that adjusts the output voltage reference accordingly.

In the sequel, we assume that the input and output voltages v_s and v_o , respectively, and the inductor current i_ℓ can be measured. The output reference voltage $v_{o,ref}$ and the current limit $i_{\ell,max}$ are given by the problem setup. Based on those measurements and parameters, the scaled quantities $v'_o, v'_{o,ref}$,

i'_ℓ and $i'_{\ell,max}$, which will be used as the inputs to the optimal controller, directly follow.

A. Objective Function

In general, the control objectives are to regulate the average output voltage to its reference as fast and with as little overshoot as possible, or equivalently, to (i) minimize the output voltage error $v'_{o,err}$ (ii) despite changes in the input voltage v_s or changes in the load resistance r_o , and (iii) to respect the constraints on the inductor current and the duty cycle. For now, we assume that the load resistance r_o is known. We will later drop this assumption.

To induce a steady state operation under a constant non-zero duty cycle, we introduce the difference between two consecutive duty cycles

$$\Delta d(k) = d(k) - d(k-1). \quad (22)$$

Next, we define the penalty matrix $Q = \text{diag}(q_1, q_2)$ with $q_1, q_2 \in \mathbb{R}^+$ and the vector $\varepsilon(k) = [v'_{o,err}(k) \ \Delta d(k)]^T$ with $v'_{o,err}(k)$ as defined in (16). Consider the objective function

$$J(x'(k), d(k-1), v'_p(k), D(k)) = \sum_{\ell=0}^{N-1} \|Q \varepsilon(k+\ell|k)\|_1, \quad (23)$$

which penalizes the predicted evolution of $\varepsilon(k+\ell|k)$ from time-instant k on over the finite horizon N using the 1-norm. Note that the objective function not only depends on the sequence of control inputs $D(k) = [d(k), \dots, d(k+N-1)]^T$ and the (measured) state $x'(k)$, but also on the last control input $d(k-1)$, the output voltage reference $v'_{o,ref}(k)$ and the current limit $i'_{\ell,max}(k)$, which are allowed to be time-varying to account for changes in the input voltage $v_s(k)$. Recall that we had defined $v'_p = [v'_{o,ref} \ i'_{\ell,max}]^T$.

Summing up, objective (i) is incorporated in the objective function, whereas objective (ii) is handled by normalizing the prediction model by v_s , feeding the model with $v'_{o,ref}$, which is basically the inverse of v_s , and assuming for now that r_o is known and updating the prediction model accordingly. Objective (iii) is easily accounted for in the prediction model, where hard constraints are imposed on the inductor current and the duty cycle.

B. On-Line Computation of Control Input

The control input at time-instant k is obtained by minimizing the objective function (23) over the sequence of control inputs $D(k)$ subject to the mixed-integer linear inequality constraints of the MLD model (17), the physical constraints on the sequence of duty cycles

$$0 \leq d(\ell) \leq 1, \quad \ell = k, \dots, k+N-1, \quad (24)$$

and the expression (22). This amounts to the CFTOC

$$D^*(k) = \arg \min_{D(k)} J(x'(k), d(k-1), v'_p(k), D(k)) \quad (25a)$$

$$\text{subj. to (17), (22), (24)} \quad (25b)$$

leading to the sequence of optimal duty cycles $D^*(k)$, of which only the first duty cycle $d^*(k)$ is applied to the

converter. At the next sampling interval, k is set to $k + 1$, a new state measurement is obtained, and the CFTOC problem is solved again over the shifted horizon according to the receding horizon policy. As we are using the 1-norm in all cost expressions, the CFTOC problem amounts to solving a *Mixed-Integer Linear Program* (MILP) for which efficient solvers exist (like [26]).

C. Off-Line Computation of State-Feedback Control Law

To allow an implementation of the proposed controller despite the high switching frequency, the solution to the CFTOC problem (25) needs to be pre-computed off-line. To do so, we use the algorithm described in [27], where the solution is generated by combining dynamic programming with multi-parametric programming and some basic polyhedral manipulations. This algorithm is based on a PWA representation of the hybrid converter model (rather than its MLD form). As in (25), the control input is parameterized by the state vector $x'(k)$, the last control input $d(k - 1)$, the output voltage reference $v'_{o,ref}(k)$ and the current limit $i'_{\ell,max}(k)$. As will be motivated in Section IV-D, we refrain from parameterizing the control law in the load, but rather assume the load resistance to be constant and nominal ($r_o = 1$ p.u.).

The resulting optimal state-feedback control law $d^*(k)$ is a PWA function of $[(x'(k))^T \ d(k - 1) \ v'_{o,ref}(k) \ i'_{\ell,max}(k)]^T$ defined on a polyhedral partition of the five-dimensional parameter space $\mathcal{X}' \times \mathcal{U} \times \mathcal{V}'$. More specifically, the state-space is partitioned into polyhedral sets and for each of these sets the optimal control law is given as an affine function of the state. For more details concerning the algorithm and the properties of its solution the reader is referred to [28].

Example 2: For the PWA model derived in Example 1 with the model and control problem parameters given in Table I, we compute the PWA state-feedback control law using the Multi-Parametric Toolbox [29]. The resulting controller is defined on 633 polyhedral regions in the five-dimensional parameter space $\mathcal{X}' \times \mathcal{U} \times \mathcal{V}'$. Using the optimal complexity reduction algorithm [30], the controller is simplified to 121 regions.

To visualize the state-feedback control law, we substitute $v'_{o,ref} = 0.556$ p.u., $i'_{\ell,max} = 1.667$ p.u. and $d(k - 1) = 0.6$ into the control law. As a result, the control law, which refers now to the nominal case, is defined on the two-dimensional state space \mathcal{X}' . Fig. 5 depicts the control input $d(k)$ as a PWA function of $x'(k)$. Note that the control law is well-defined, that is for each $x'(k) \in \mathcal{X}'$, $d(k - 1) \in \mathcal{U}$ and $v'_p(k) \in \mathcal{V}'$ exists a polyhedron and an associated affine control law such that $d(k)$ can be evaluated as can be seen from Fig. 5(b). Yet, the control law is discontinuous leading to the gaps visible in Fig. 5(a).

This control law, which is essentially a collection of (affine) proportional (P) controllers, can be interpreted as follows. In a small neighborhood of the steady state operating point, which is given by $i'_\ell = 0.3011$ p.u., $v'_o = 0.556$ p.u. and $d(k) = 0.585$ p.u., the controller resembles an affine P-controller. Further away from the operating point the behavior of the controller changes drastically. In particular, the control law saturates to respect the $[0, 1]$ constraint on the duty cycle and

achieve optimality with respect to the objective function (23). For very small (and very high) output voltages, the upper (and lower) current constraint becomes active. This is reflected in the 'bending' of the control law visible in Fig. 5.

D. Load Variations

In the following, we drop the assumption that the load resistance is known and time-invariant. The load might be estimated (e.g. by using an extended Kalman filter), but as can be seen from (8), the load enters the model equations nonlinearly. To account for that, numerous PWA approximations would be necessary leading to an overly complex PWA model and an extremely complex state-feedback control law. We rather aim at a way to cope with load changes without introducing too much additional complexity. Hence, we propose to use the previously derived state-feedback controller (for a time-invariant and nominal load $r_o = 1$), to which we add a loop.

As can be seen from (8), in general, changes in the load resistor affect the converter dynamics and the dc gain. This is particularly the case, when the load decreases significantly below the nominal value. Yet, in the presence of extreme load resistor drops when the current constraint becomes active, the only objective of the controller is to respect the safety constraint on the inductor current and to drop the output voltage accordingly. On the other hand, if the load is roughly nominal or increased beyond its nominal value, then the dynamics and the dc gain are subject only to minor changes. Yet, due to the accuracy requirement for the output voltage regulation (steady state error below 0.5 %), even small errors in the dc gain need to be addressed. We suggest to cope with this issue by adjusting the scaled output voltage reference fed into the controller such that the error between the output voltage and the *actual* reference is made small.

This can be achieved through the use of a Kalman filter [31] that yields a zero steady-state output voltage error due to its integrating character. For this, we augment the reformulated (nominal) continuous-time system (8)–(11) by a third state v'_e that tracks the output voltage error, and we use the Kalman filter to estimate the augmented state vector

$$x'_a = [i'_\ell \ v'_o \ v'_e]^T. \quad (26)$$

The augmented model is modelled with a stochastic continuous-time state equation

$$\frac{dx'_a(t)}{dt} = \begin{bmatrix} F & 0 \\ 0 & 0 \end{bmatrix} x'_a(t) + \begin{bmatrix} f \\ 0 \end{bmatrix} u(t) + Gw_1(t), \quad (27)$$

where $u(t)$ is the signal that drives the converter's primary switch

$$u(t) = \begin{cases} 1, & kT_s \leq t < (k + d(k))T_s \\ 0, & (k + d(k))T_s \leq t < (k + 1)T_s \end{cases} \quad (28)$$

and the measurement equation

$$\begin{bmatrix} i'_\ell(t) \\ v'_o(t) \end{bmatrix} = \begin{bmatrix} 1 & 0 & 0 \\ 0 & 1 & 1 \end{bmatrix} x'_a(t) + Hw_2(t), \quad (29)$$

with the matrices $G = \text{diag}(1, 1, 1)$ and $H = \text{diag}(1, 1)$. The random variables $w_1(t) \in \mathbb{R}^3$ and $w_2(t) \in \mathbb{R}^2$ represent the process and the measurement noise, respectively. They are

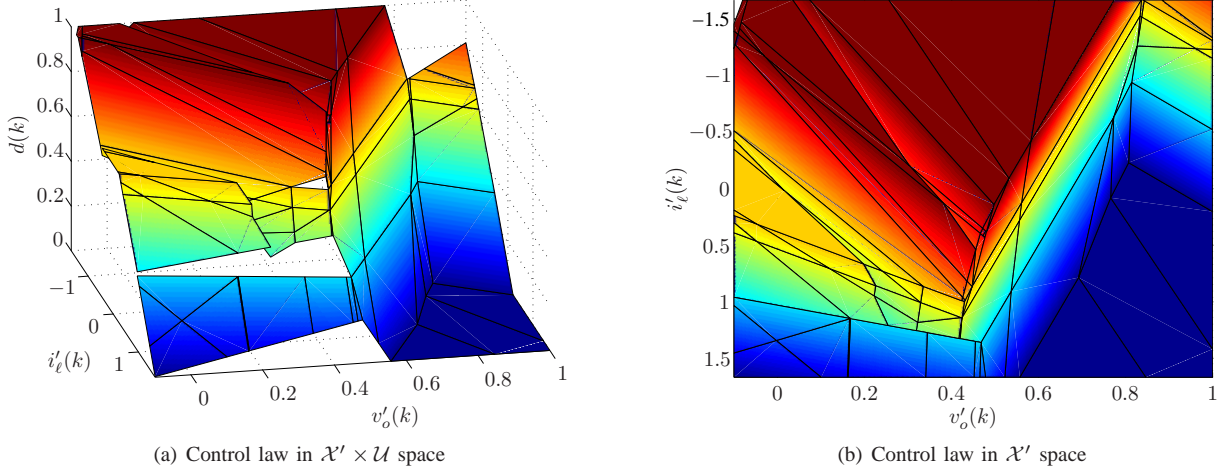


Fig. 5: State-feedback control law $d(k)$ for $d(k-1) = 0.6$, $v'_{o,ref} = 0.556$ p.u. and $i'_{\ell,max} = 1.667$ p.u., where dark blue corresponds to $d(k) = 0$ and dark red to $d(k) = 1$

independent white and normal (Gaussian) probability distributions with $E[w_1 w_1^T] = W_1$, $E[w_2 w_2^T] = W_2$ and $E[w_1 w_2^T] = 0$, where 0 is a zero matrix of appropriate dimension. We require $GW_1 G^T \succeq 0$ and $W_2 + HW_1 H^T \succ 0$. Note that the augmented model is detectable and uses the nominal value of the load resistor. Moreover, the effects of the switching in the converter are lumped in the time-varying input at the right-hand side of (27), thus reducing the estimation problem to that of a linear system driven by a time-varying input.

To allow an easy implementation of the Kalman filter, we use a steady-state constant Kalman gain. To calculate this, the noise covariance matrices W_1 and W_2 are chosen such that high credibility is assigned to the measurements and dynamics of the physical states, namely i'_ℓ and v'_o , while low credibility is assigned to the dynamics of the dummy state v'_e . As a result, the Kalman filter accurately tracks the physical states, while the error due to the model mismatch (coming e.g. from the different loads) is assigned to v'_e . As a result, the third state v'_e tracks the output voltage error. In a last step, we adjust the output voltage reference $v'_{o,ref}$ by the tracked voltage error. Specifically, we replace $v'_{o,ref}$ in (10) by

$$\tilde{v}'_{o,ref} = v'_{o,ref} - \hat{v}'_e, \quad (30)$$

where \hat{v}'_e denotes the estimate of v'_e .

V. ANALYSIS

In an a posteriori analysis, we aim to show – by deriving a piecewise quadratic (PWQ) Lyapunov function [32] – that the optimal controller leads to exponential closed-loop stability. Starting with the explicit PWA representation of the optimal control law, we close the control loop with the PWA ν -resolution model derived in Section III-C.2. This leads to a closed-loop system, which is PWA and autonomous by definition. To facilitate the analysis, we restrict ourselves to the nominal case with nominal load and nominal input voltage, namely $r_o = 1$ p.u. and $v_s = 1.8$ p.u.. Hence, a Kalman filter adjusting the output voltage reference is obsolete and the output voltage reference is constant.

Let $x'_c(k) = [i'_\ell(k) \ v'_o(k) \ d(k-1)]^T$, $x'_c(k) \in \mathcal{X}' \times \mathcal{U}$ denote the state vector of the autonomous system, and assume that an equilibrium point \bar{x}'_c exists for $\bar{v}'_o = v'_{o,ref}$. Since we aim at showing stability of the equilibrium point \bar{x}'_c , we perform the coordinate transformation

$$\zeta(k) = x'_c(k) - \bar{x}'_c. \quad (31)$$

In the sequel, we consider the autonomous system with state vector $\zeta(k) \in \mathcal{Z}$, $\mathcal{Z} = \{\zeta \mid \zeta + \bar{x}'_c \in \mathcal{X}' \times \mathcal{U}\}$. For this system, consider the invariant subset $\mathcal{Z}_0 \subseteq \mathcal{Z}$ defined as

$$\mathcal{Z}_0 = \{\zeta(0) \in \mathcal{Z} \mid \zeta(k) \in \mathcal{Z} \ \forall k \geq 0\}. \quad (32)$$

We adopt the PWQ function

$$L(\zeta) = \zeta^T P_i \zeta \quad \text{if } \zeta \in \mathcal{Q}_i, \quad (33)$$

where P_i is a constant 3×3 matrix and \mathcal{Q}_i is a polyhedron. We impose

$$L(\zeta(k)) \geq \varrho_i \|\zeta(k)\|_2^2 \quad \forall \zeta(k) \in \mathcal{Q}_i \cap \mathcal{Z}_0 \quad (34)$$

and

$$L(\zeta(k+1)) - L(\zeta(k)) \leq -\rho \|\zeta(k)\|_2^2 \quad \forall \zeta(k) \in \mathcal{Z}_0, \quad (35)$$

where $\varrho_i > 0$ and $\rho > 0$. Note that (34) does not imply that the matrices P_i are positive definite since the inequalities are required to hold only for the corresponding i -th polyhedron. Furthermore, $L(\zeta)$ may be discontinuous across the polyhedral boundaries.

Theorem 1: [32, Theorem 1] The equilibrium $\zeta = 0$ of the above autonomous system is exponentially stable on \mathcal{Z}_0 if there exists a PWQ Lyapunov function $L(\zeta)$ as in (33)–(35). For details on Lyapunov functions for PWA systems and computation approaches, the reader is referred to [32] and [33], respectively.

Example 3: Consider the nominal ν -resolution model in PWA form as in Example 1 (with the nominal parameters as in Table I), and the corresponding state-feedback control law derived in Example 2. An analysis shows that an equilibrium

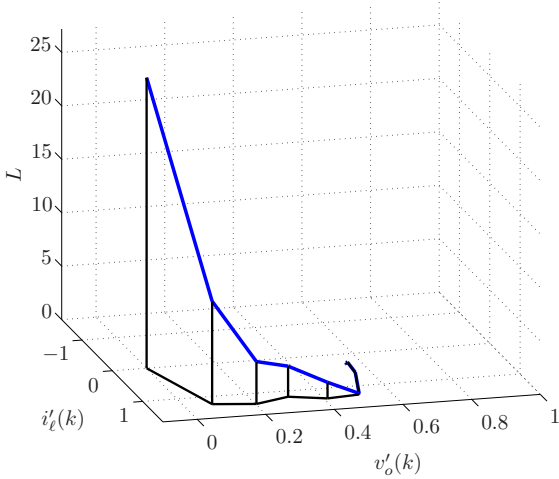


Fig. 6: Value of Lyapunov function along closed-loop trajectory during start-up plotted on the \mathcal{X}' plane

point \bar{x}'_c with $\bar{v}'_o = v'_{o,ref}$ exists. This allows the derivation of the closed-loop autonomous system with state vector $\zeta(k) \in \mathcal{Z}$. A subsequent evaluation of the autonomous system shows that the control invariant subset is equal to $\mathcal{X}' \times \mathcal{U}$, and consequently $\mathcal{Z}_0 = \mathcal{Z}$. This implies that for any initial state within $\mathcal{X}' \times \mathcal{U}$, all constraints will be met at all future time-instants. In particular, a control input will always be found.

Using the Multi-Parametric Toolbox [29], a PWQ Lyapunov function $L(\zeta)$ with $\rho = 3.4 \cdot 10^{-5}$ is found in 2.9 min on a 2.8 GHz Pentium IV machine. Consequently, the nominal closed-loop system is exponentially stable. We would like to stress that stability is proven for all $x'_c(k) \in \mathcal{X}' \times \mathcal{U}$ and not only locally around $v'_{o,ref}$. This is in contrast to classic stability analysis techniques based on a linearized model that allow proving stability only in a (small) neighborhood around the operating point.

For the nominal start-up, the decaying value of the Lyapunov function along the closed-loop trajectory $x'_c(k)$, $k \in \mathbb{N}_0$, is depicted in Fig. 6. In this figure, $L(x'_c(k) - \bar{x}'_c)$ is plotted over the two-dimensional state-space \mathcal{X}' , where the third dimension corresponding to $d(k-1) \in \mathcal{U}$ has been omitted. Note that for \mathcal{X}' the same scaling is used as in Fig. 5 to allow a direct comparison.

VI. SIMULATION RESULTS

In this section, simulation results demonstrating the potential advantages of the proposed control methodology are presented. Specifically, we examine the closed-loop dynamical behavior for the start-up, and the response to step changes in the input voltage and the load resistance, respectively. The simulations were carried out using the continuous-time nonlinear model of the converter (1)–(7) as the real plant, closing the loop with the constrained optimal controller designed in Section IV. The inductor current of the converter and the input and output voltages were regarded to be measurable as it is current industrial practice. Furthermore, we neglected measurement noise. All variables in the following figures are

Parameters of the Converter					
x_c	10.294 p.u.	x_ℓ	0.477 p.u.	$i_{\ell,max}$	3 p.u.
r_c	0.001 p.u.	r_ℓ	0.05 p.u.	r_o	1 p.u.
Parameters of the Controller					
ν	3	N	2		
q_1	4	q_2	0.1		

TABLE I: Model and controller parameters used for the simulation results

normalized to the *per unit* system, and one time unit of the time axis equals one switching period.

The circuit parameters of the converter are summarized in Table I. The parameters were chosen to represent a realistic problem set-up, describing for example a 24 V to 12 V, 144 W synchronous step-down converter operating with a switching frequency of 100 kHz. If not stated otherwise, the input voltage is $v_s = 1.8$ p.u. and the output resistance is given by $r_o = 1$ p.u.. The output voltage reference is $v_{o,ref} = 1$ p.u..

The ν -resolution model uses the same parameters as the physical plant model, with the difference that it is scaled with respect to v_s and that it always uses the nominal load $r_o = 1$ p.u.. Even though two subperiods ν in the ν -resolution modelling approach yield satisfactory results, we chose $\nu = 3$ to accurately model the nonlinear dynamics. The polyhedral partition of the PWA model is visualized in Fig. 3.

Regarding the optimal control scheme, the penalty matrix is chosen to be $Q = \text{diag}(4, 0.1)$, putting a rather small weight on the changes of the manipulated variable. In all simulations, the prediction horizon is set to $N = 2$. Based on this, as detailed in Section IV-C and Example 2, the PWA state-feedback control law shown in Fig. 5 is derived for the nominal output resistance $r_o = 1$ p.u..

For the covariance matrices of the Kalman filter, we set $W_1 = \text{diag}(0.1, 0.1, 100)$ and $W_2 = \text{diag}(1, 1)$. These are the same both for the on and the off mode (corresponding to S_1 being on and off, respectively).

A. Nominal Start-Up

Fig. 7 shows the step responses of the converter in nominal operation during start-up with the initial state $x(0) = [0 \ 0]^T$ and $d(-1) = 0$. The following three control schemes are compared: MPC with a $\nu = 3$ resolution model, MPC with an averaged model ($\nu = 1$) and the industrial standard – a current mode control scheme. Since the latter is known to be unstable for duty cycles above 0.5 [34], we have included a slope compensation scheme to remove this instability. This addition and the tuning of the PI controller is done following the design procedure summarized in [34].

For MPC with the $\nu = 3$ resolution model the output voltage reaches its steady state within ten switching periods with an overshoot not exceeding 3%. As can be seen the current constraint is largely respected. The small violations are due to the coarse resolution of the ν -resolution model. Specifically, the current constraint can only be imposed at ν time-instants within the switching period. The steady state error in the output voltage is with 0.5% sufficiently small and can be further reduced by increasing ν .

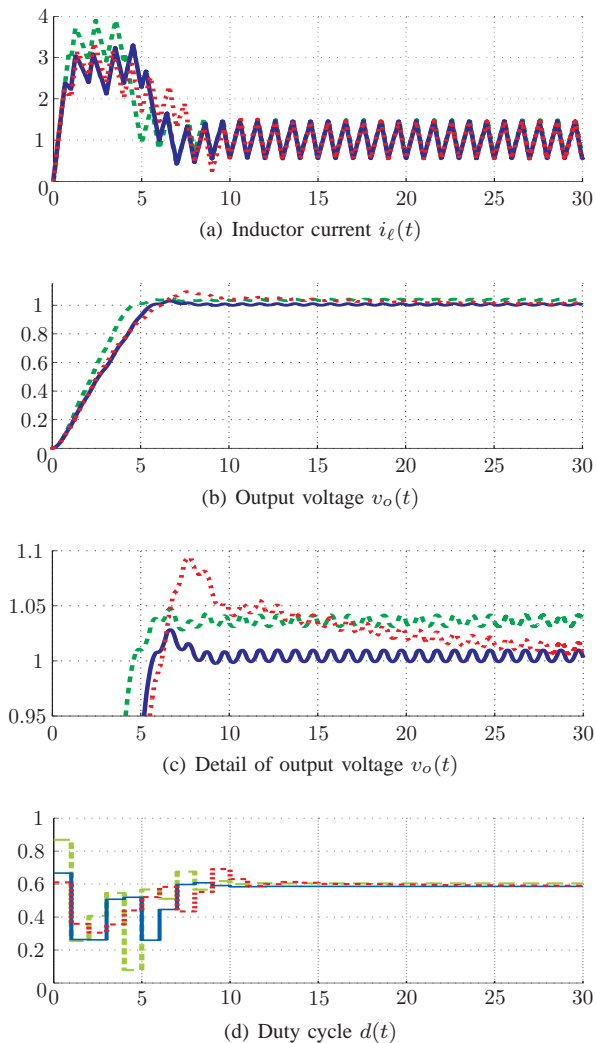


Fig. 7: Closed-loop responses during start-up in nominal operation for MPC with $\nu = 3$ resolution model (solid blue lines), MPC with averaged model (dashed green lines), and current mode PI controller (dotted red lines)

The MPC scheme using the averaged model with $\nu = 1$ leads to a steady state output error of 3.5%. Moreover, the current constraint is violated by up to 30%, thus making a shorter rise time possible. The inaccurate averaged model motivates the use of a hybrid model with $\nu > 1$. The current mode PI controller, on the other hand, respects the current constraint and yields the same rise time as MPC with the $\nu = 3$ resolution model. Yet, it exhibits a large overshoot of almost 10% and a large settling time of approximately 30 switching periods.

B. Step Changes in Input Voltage

Operating at steady state with the nominal input voltage $v_s = 1.8$ p.u. a step change down to $v_s = 1.2$ p.u. occurs at time-instant $k = 3.5$. The closed-loop disturbance responses for MPC with the $\nu = 3$ resolution model and for the current mode PI controller are shown in Fig. 8. In contrast to the PI controller, MPC rejects the disturbance well. Specifically, the output voltage remains practically unaffected and the controller settles at the new steady-state duty cycle very quickly

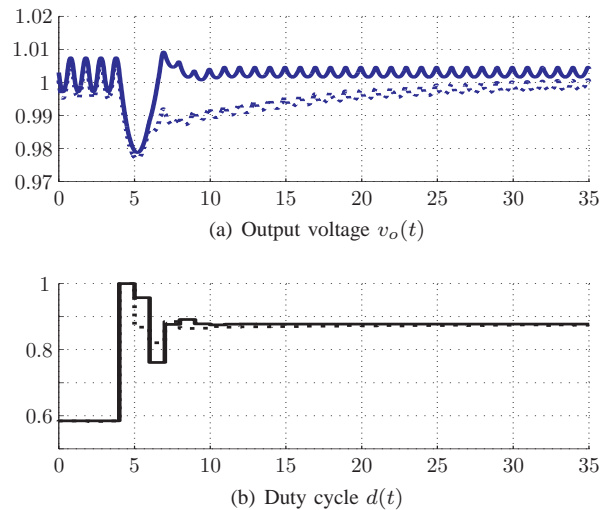


Fig. 8: Closed-loop response to a step-down change in the input voltage from $v_s = 1.8$ p.u. to $v_s = 1.2$ p.u. at time-instant $k = 3.5$ for MPC with $\nu = 3$ resolution model (solid lines) and current mode PI controller (dotted lines)

within four switching periods. The relatively large undershoot results from the constraint $d(k) \leq 1$, as can be seen in Fig. 8. Step-up changes in the input voltage lead to similar results. The step-up case from $v_s = 1.8$ p.u. to $v_s = 3$ p.u. can be found in [2].

Summing up, disturbances in the input voltage are rejected very effectively by the controller, and the output voltage is quickly restored to its reference. This is because the state-feedback control law is indirectly parameterized by the input voltage by scaling the measured states, the output voltage reference and the current limit with respect to v_s . As a result, the performance of the controller is not affected by changes in v_s .

C. Step Changes in Output Resistance

In a last step, we investigate the closed-loop performance in the presence of major step changes in the output resistance r_o . In the sequel, we add the Kalman filter to the MPC controller, where the Kalman filter is used to adjust the output voltage reference $v'_{o,ref}$ to account for unmeasured changes in r_o .

Starting from the nominal load $r_o = 1$ p.u., at time-instant $k = 3.5$, a step down to $r_o = 0.5$ p.u. is applied. Fig. 9 depicts the corresponding closed-loop performance for MPC and the current mode PI controller. As can be observed, the dynamic behavior of MPC is superior to the PI controller leading to a three times smaller settling time. Step-up changes in the output resistance lead to similar results. The step-up case from $r_o = 1$ p.u. to $r_o = 4$ p.u. can be found in [2].

In the last case, we examine a crucial aspect of the controller operation, namely the system's protection against excessive load currents. Aiming at activating the current constraint, the load drops at $k = 3.5$ from its nominal value to $r_o = 0.05$ p.u. basically creating a short circuit at the output. The simulation results in Fig. 10 show that the proposed controller respects the current limit and forces the output voltage v_o to drop to the level that is needed to respect the constraint. We would like to stress that this feature is explicitly addressed

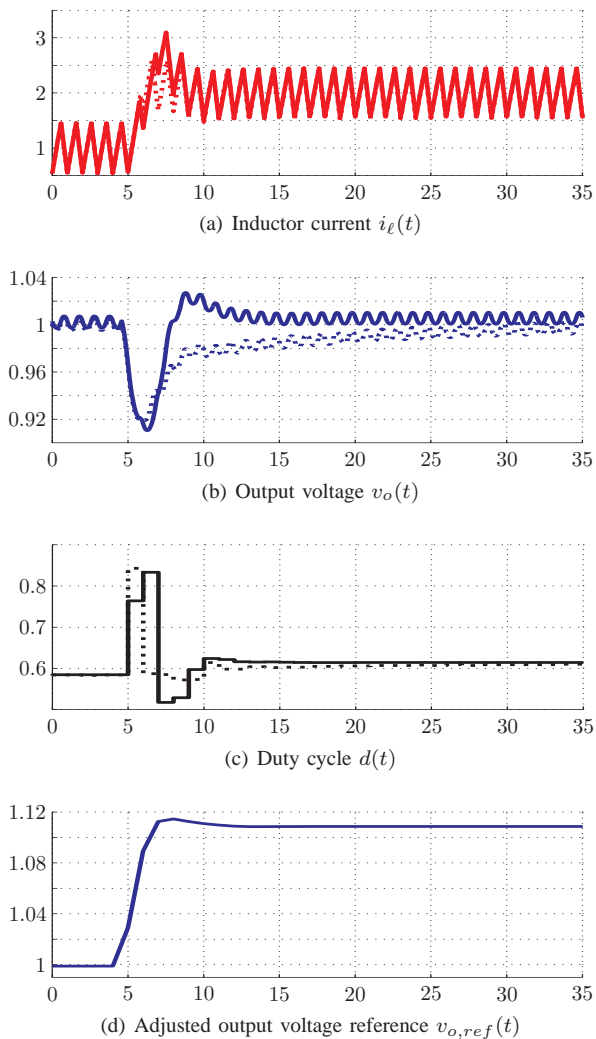


Fig. 9: Closed-loop response to a step-down change in the load resistor from $r_o = 1$ p.u. to $r_o = 0.5$ p.u. at time-instant $k = 3.5$. The solid lines correspond to MPC with a Kalman filter, the dotted lines to the current mode PI controller

during the controller design by simply adding the current constraint to control problem formulation. This is in contrast to the classic PI controller design procedure, where a current limiting protection scheme is not directly treated as part of the controller design.

As anticipated in Section IV-D, the Kalman filter and the inaccuracy introduced by the usage of the nominal r_o are overshadowed by the presence of the current constraint. Hence, for small changes in r_o , a Kalman filter is needed for achieving a zero steady-state error – possibly causing a slight deterioration of the dynamic performance. Yet for large load drops, due to the activation of the current constraint, the Kalman filter has hardly any effect on the closed-loop dynamic behavior. In particular, the Kalman filter does not lead to violations of this constraint. This argument justifies the reasoning in Section IV-D, where we proposed the use of the nominal ν -resolution model with $r_o = 1$ p.u. in combination with a Kalman filter.

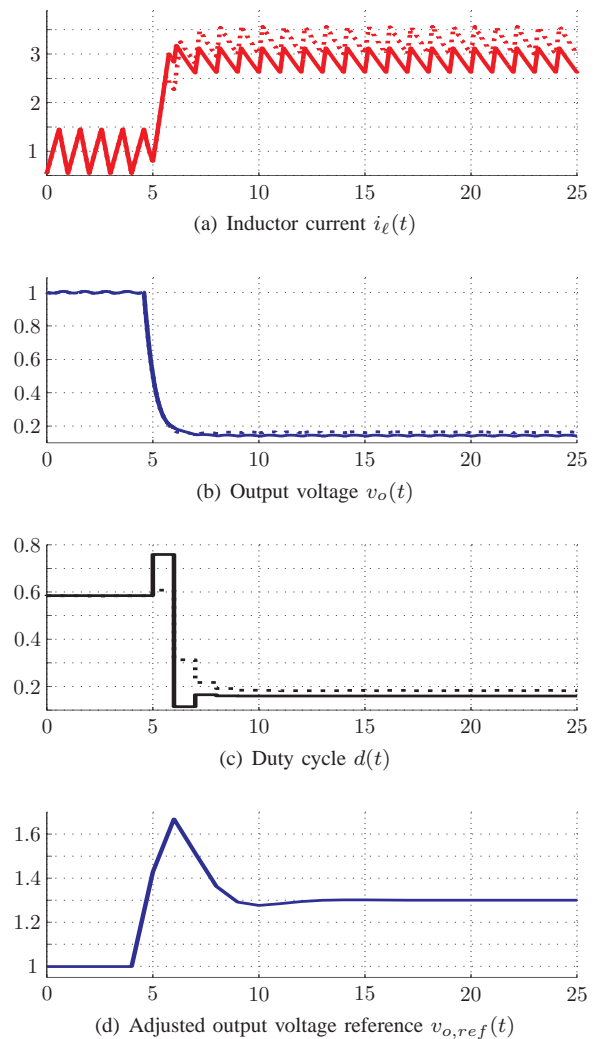


Fig. 10: Closed-loop response to a short circuit (the load resistance is reduced from $r_o = 1$ p.u. to $r_o = 0.05$ p.u.) at time-instant $k = 3.5$. The solid lines correspond to MPC with a Kalman filter, the dotted lines to the current mode PI controller

VII. CONCLUSIONS

We have presented a new modelling and control approach for fixed frequency switch-mode dc-dc converters by formulating a constrained optimal control problem using hybrid systems methodologies. The method is presented here for synchronous step-down dc-dc converters, but as shown in [35] and [36], it is directly extendable to other converter topologies of the same class.

More specifically, for the synchronous step-down converter, a novel ν -resolution hybrid model was introduced to avoid averaging and to model the converter arbitrarily accurately, and a constrained finite time optimal control problem was formulated and solved online and off-line. This control methodology enabled us to explicitly take into account during the design phase physical constraints, such as the restriction of the duty cycle between zero and one, and safety constraints, such as current limiting. The off-line solution to the control problem yielded an explicit state-feedback controller defined on a polyhedral partition of the state-space that allows the practical

implementation of the proposed scheme.

This controller is parameterized not only by the measured states $i'_\ell(k)$ and $v'_o(k)$, which are scaled by the input voltage v_s , and the previous duty cycle $d(k-1)$, but also by the scaled output voltage reference $v'_{o,ref}(k)$ and the scaled current limit $i'_{\ell,max}(k)$. This allowed us to efficiently reject disturbances in the input voltage of any magnitude. Moreover, the addition of a Kalman filter estimating the output voltage error and adjusting the voltage reference accordingly provides disturbance rejection to large changes in the output resistance. These include short circuits, for which the output voltage is dropped such that the safety constraint is respected. Most importantly, the control invariant set was derived proving that the controller renders the nominal system exponentially stable. Simulation results have been provided demonstrating that the proposed controller leads to a closed-loop system with very favorable dynamical properties.

VIII. ACKNOWLEDGEMENTS

This work was supported by the two European Commission research projects IST-2001-33520 *Control and Computation (CC)* and FP6-IST-511368 *Hybrid Control (HYCON)*.

REFERENCES

- [1] D. P. Bertsekas, *Dynamic Programming and Optimal Control*. Athena Scientific, 1995.
- [2] T. Geyer, "Low complexity model predictive control in power electronics and power systems," Dr. sc. tech. thesis, Automatic Control Laboratory ETH Zurich, 2005.
- [3] R. D. Middlebrook and S. Čuk, "A general unified approach to modeling switching power converter stages," 1976, pp. 18–34.
- [4] R. W. Erickson, S. Čuk, and R. D. Middlebrook, "Large signal modeling and analysis of switching regulators," 1982, pp. 240–250.
- [5] T. Gupta, R. R. Boudreaux, R. M. Nelms, and J. Y. Hung, "Implementation of a fuzzy controller for DC-DC converters using an inexpensive 8-b microcontroller," *IEEE Trans. Ind. Electron.*, vol. 44, no. 5, pp. 661–669, Oct. 1997.
- [6] F. Garofalo, P. Marino, S. Scala, and F. Vasca, "Control of DC/DC converters with linear optimal feedback and nonlinear feedforward," *IEEE Trans. Power Electron.*, vol. 9, no. 6, pp. 607–615, Nov. 1994.
- [7] H. Sira-Ramírez, "Nonlinear P-I controller design for switchmode DC-to-DC power converters," *IEEE Trans. Circuits Syst. I*, vol. 38, no. 4, pp. 410–417, Apr. 1991.
- [8] S. R. Sanders and G. C. Verghese, "Lyapunov-based control for switched power converters," *IEEE Trans. Power Electron.*, vol. 7, no. 1, pp. 17–23, Jan. 1992.
- [9] S. Hiti and D. Borojevic, "Robust nonlinear control for the boost converter," *IEEE Trans. Power Electron.*, vol. 10, no. 6, pp. 651–658, Nov. 1995.
- [10] M. K. Kazimierczuk and A. Massarini, "Feedforward control dynamic of DC/DC PWM boost converter," *IEEE Trans. Circuits Syst. I*, vol. 44, no. 2, pp. 143–149, Feb. 1997.
- [11] M. K. Kazimierczuk and L. A. Starman, "Dynamic performance of PWM DC/DC boost converter with input voltage feedforward control," *IEEE Trans. Circuits Syst. I*, vol. 46, no. 12, pp. 1473–1481, Dec. 1999.
- [12] F. H. F. Leung, P. K. S. Tam, and C. K. Li, "The control of switching DC-DC converters – a general LQR problem," *IEEE Trans. Ind. Electron.*, vol. 38, no. 1, pp. 65–71, Feb. 1991.
- [13] —, "An improved LQR-based controller for switching DC-DC converters," *IEEE Trans. Ind. Electron.*, vol. 40, no. 5, pp. 521–528, Oct. 1993.
- [14] M. Lazar and R. De Keyser, "Non-linear predictive control of a dc-to-dc converter," in *Symposium on Power Electronics, Electrical Drives, Automation and Motion*, Capri, Italy, 2004.
- [15] D. W. Clarke, C. Mohtadi, and P. S. Tuffs, "Generalized predictive control – part I. The basic algorithm," *Automatica*, vol. 23, no. 2, pp. 137–148, 1987.
- [16] B. Lincoln, "Dynamic programming and time-varying delay systems," Ph.D. dissertation, Department of Automatic Control, Lund Institute of Technology, Lund, Sweden, 2003.
- [17] J. Buisson, P.-Y. Richard, and H. Cormerais, "On the stabilisation of switching electrical power converters," in *Hybrid Systems: Computation and Control*, ser. LNCS, M. Morari and L. Thiele, Eds. Springer, 2005, vol. 3414, pp. 184–197.
- [18] S. Almér, U. Jönsson, C.-Y. Kao, and J. Mari, "Global stability analysis of dc-dc converters using sampled-data modeling," in *Proc. American Control Conf.*, Boston, MA, June 2004, pp. 4549–4554.
- [19] F. D. Torrisi and A. Bemporad, "Hysdel — a tool for generating computational hybrid models for analysis and synthesis problems," *IEEE Trans. Contr. Syst. Technol.*, vol. 12, no. 2, pp. 235–249, Mar. 2004.
- [20] A. Bemporad and M. Morari, "Control of systems integrating logic, dynamics and constraints," *Automatica*, vol. 35, no. 3, pp. 407–427, March 1999.
- [21] E. D. Sontag, "Nonlinear regulation: The piecewise linear approach," *IEEE Trans. Automat. Contr.*, vol. 26, no. 2, pp. 346–358, Apr. 1981.
- [22] W. P. M. H. Heemels, B. De Schutter, and A. Bemporad, "Equivalence of hybrid dynamical models," *Automatica*, vol. 37, no. 7, pp. 1085–1091, July 2001.
- [23] T. Geyer, F. D. Torrisi, and M. Morari, "Efficient mode enumeration of compositional hybrid systems," in *Hybrid Systems: Computation and Control*, ser. LNCS, A. Pnueli and O. Maler, Eds. Springer, 2003, vol. 2623, pp. 216–232.
- [24] J. Maciejowski, *Predictive Control*. Prentice Hall, 2002.
- [25] F. Borrelli, *Constrained Optimal Control of Linear and Hybrid Systems*, ser. LNCIS. Springer, 2003, vol. 290.
- [26] ILOG, Inc., *CPLEX 8.0 User Manual*, Gentilly Cedex, France, 2002.
- [27] M. Baotić, F. J. Christophersen, and M. Morari, "A new algorithm for constrained finite time optimal control of hybrid systems with a linear performance index," in *Proc. of the European Control Conf.*, Cambridge, UK, Sept. 2003.
- [28] F. Borrelli, M. Baotić, A. Bemporad, and M. Morari, "Dynamic programming for constrained optimal control of discrete-time linear hybrid systems," *Automatica*, vol. 41, no. 10, pp. 1709–1721, Oct. 2005.
- [29] M. Kvasnica, P. Grieder, M. Baotić, and M. Morari, "Multi parametric toolbox (MPT)," in *Hybrid Systems: Computation and Control*, ser. LNCS, R. Alur and G. Pappas, Eds. Springer, 2004, vol. 2993, pp. 448–462, <http://control.ee.ethz.ch/~mpt>.
- [30] T. Geyer, F. D. Torrisi, and M. Morari, "Optimal complexity reduction of piecewise affine models based on hyperplane arrangements," in *Proc. American Control Conf.*, Boston, MA, June 2004, pp. 1190–1195.
- [31] A. H. Jazwinski, *Stochastic Processes and Filtering Theory*. Academic Press, 1970.
- [32] G. Ferrari-Trecate, F. A. Cuzzola, D. Mignone, and M. Morari, "Analysis of discrete-time piecewise affine and hybrid systems," *Automatica*, vol. 38, no. 12, pp. 2139–2146, March 2002.
- [33] P. Grieder, M. Lüthi, P. Parrilo, and M. Morari, "Stability & feasibility of constrained receding horizon control," in *Proc. of the European Control Conf.*, Cambridge, UK, Sept. 2003.
- [34] D. Mitchell and B. Mammano, "Designing stable control loops," Unirode Design Seminars, 2001, <http://focus.ti.com/lit/ml/slup173/slup173.pdf>.
- [35] A. G. Beccuti, G. Papafotiou, and M. Morari, "Explicit model predictive control of the boost dc-dc converter," in *Proceedings of the 2nd IFAC Conf. on Analysis and Design of Hybrid Systems*, Alghero, Italy, 2006.
- [36] —, "Optimal control of the buck dc-dc converter operating in both the continuous and discontinuous conduction regimes," in *Proc. 45th IEEE Conf. on Decision and Control*, San Diego, California, USA, Dec. 2006.